Available online at www.sciencedirect.com

SciVerse ScienceDirect

Geochimica et Cosmochimica Acta 75 (2011) 6570–6583

Geochimica et Cosmochimica Acta

www.elsevier.com/locate/gca

Trace element partitioning in the Fe–S–C system and its implications for planetary differentiation and the thermal history of ureilites

Leslie A. Hayden [a,*], James A. Van Orman [a], William F. McDonough [b], Richard D. Ash [b], Cyrena A. Goodrich [c]

[a] Department of Geological Sciences, Case Western Reserve University, 10900 Euclid Ave., Cleveland, OH 44106, USA
[b] Department of Geology, University of Maryland, College Park, MD 20742, USA
[c] Planetary Science Institute, 1700 E. Ft. Lowell Dr., Tucson, AZ 85719, USA

Received 14 December 2010; accepted in revised form 25 August 2011; available online 31 August 2011

Abstract

Element partitioning in metal–light element systems is important to our understanding of planetary differentiation processes. In this study, solid-metal/liquid-sulfide, liquid-metal/liquid-sulfide and solid-metal/troilite partition coefficients (D) were determined for 18 elements (Ag, As, Au, Co, Cr, Cu, Ge, Ir, Ni, Os, Pd, Pt, Mo, Mn, Re, Ru, Se and W) in the graphite-saturated Fe–S–C system at 1 atm. Compared at the same liquid S concentration, the solid/liquid partition coefficients are similar to those in the Fe–S system, but there are systematic differences that appear to be related to interactions with carbon dissolved in the solid metal. Elements previously shown to be "anthracophile" generally have larger solid/liquid partition coefficients in the Fe–S–C system, whereas those that are not have similar or smaller partition coefficients in the Fe–S–C system. The partitioning of trace elements between C-rich and S-rich liquids is, in most cases, broadly similar to the partitioning between solid metal and S-rich liquid. The highly siderophile elements Os, Re, Ir and W are partitioned strongly into the C-rich liquid, with $D \gg 100$. The partition coefficients for Pt, Ge and W decrease significantly at the transition to liquid immiscibility, while the partition coefficient for Mo increases sharply. The bulk siderophile element patterns of ureilite meteorities appear to be better explained by separation of S-rich liquid from residual C-rich metallic liquid at temperatures above the silicate solidus, rather than by separation of S-rich liquid from residual solid metal at lower temperatures.

1. INTRODUCTION

Element partitioning in metal alloy systems that contain light elements is important to our understanding of planetary differentiation processes. Partitioning of elements between solid and liquid alloys leads to chemical fractionation during the progressive solidification of asteroidal and planetary cores. Interpreting the chemical trends preserved in iron meteorites (e.g., Kelly and Larimer, 1977; Haack and Scott, 1993; Chabot et al., 2003; Walker et al., 2008), and predicting the chemical and isotopic signatures that may result from crystallization of Earth's inner core (Brandon and Walker, 2005), both rely on understanding the fundamental controls on element partitioning in solid/liquid iron alloy systems. It is also important to understand how elements are partitioned between immiscible liquids and among solid iron alloys, sulfides, carbides and phosphides, all of which may be present during the late stages of core solidification and sub-solidus evolution.

Element partitioning in iron alloy systems also could lead to significant fractionation during the early stages of

* Corresponding author. Present address: Department of Geological Sciences, University of Michigan, 2534 C.C. Little Bldg., 1100N. University Ave., Ann Arbor, MI 48109, USA. Tel.: +1 734 615 2048; fax: +1 734 763 4690.
E-mail addresses: lahayden@umich.edu (L.A. Hayden), jav12@case.edu (J.A. Van Orman).

0016-7037/$ - see front matter © 2011 Elsevier Ltd. All rights reserved.
doi:10.1016/j.gca.2011.08.036

melting and core formation in planetesimals. For example, in ureilites, one of the major groups of primitive achondritic meteorites, the relative abundances of siderophile and chalcophile elements has been explained by the extraction of a sulfur-rich metallic liquid, leaving behind iron-rich metal (Janssens et al., 1987; Warren et al., 2006; Rankenburg et al., 2008).

There have been numerous studies of partitioning in solid-metal/liquid-metal systems, which have demonstrated that the presence of a single light element such as S, C, or P can strongly influence the trace element partitioning behavior (e.g., Jones et al., 1993; Fleet et al., 1999; Chabot and Drake, 2000; Liu and Fleet, 2001; Chabot et al., 2003, 2006, 2008; Corrigan et al., 2009). Sulfur and carbon in particular have been the focus of several studies, because these elements are common in iron meteorites and are plausible candidates as light alloying element(s) in Earth's core (e.g., Wood, 1993; Li and Agee, 1996, 2001; Li et al., 2001). These studies have shown that the partition coefficients for trace elements between solid metal and liquid metal are a strong function of the S or C concentration of the liquid, and can be described as a power law function of the molar fraction of metallic species (Fe domains) in the liquid (Chabot and Jones, 2003; Chabot et al., 2006, 2008). However, the magnitude of the dependence of the trace element partition coefficient on liquid composition is generally not the same for C- and S-bearing systems, and may not even have the same sign. Tungsten, for example, is strongly repelled by S in the liquid (Lauer et al., 2001; Chabot and Jones, 2003) but is attracted by C in the liquid (Chabot et al., 2006). It is not obvious how to predict the simultaneous influence of S and C on trace element partition coefficients in multi-component metallic systems, particularly since C can have significant abundances in both solid and liquid phases, while S is strongly concentrated in the liquid only.

Here we present the results of an experimental study on trace element partitioning in the Fe–S–C system, over a broad range of temperatures encompassing sub-solidus conditions to the regime of C-rich liquid/S-rich liquid immiscibility. All experiments were conducted under graphite-saturated conditions, making the system invariant at fixed pressure and temperature; i.e., in each experiment there are zero degrees of freedom and the compositions of all phases at equilibrium are fixed. The experimental results are directly applicable to ureilites, in which graphite is ubiquitous (Goodrich, 1992 and refs. therein). Our results also provide a basis for the calibration of a thermodynamic model that can be extended to predict trace element partition coefficients in the Fe–S–C system under non-graphite-saturated conditions (Van Orman and Hayden, 2011).

2. EXPERIMENTAL AND ANALYTICAL METHODS

The experiments were conducted in sealed silica glass capsules held within a 1-atmosphere Sentro Tech box furnace at Case Western Reserve University. Starting powders were mixed from commercially available powders of Fe and FeS, with trace elements added at a concentration of approximately 200–500 ppm each from high-purity powders of Ag, As, Au, Co, Cr, Cu, Ge, Ir, Mn, Mo, Ni, Os, Pd, Pt, Re, Ru, Se and W. Two starting bulk compositions were used, $Fe_{64}S_{36}$ (975–1175 °C) and $Fe_{82}S_{18}$ (1200–1350 °C). For each experiment, about 100 mg of the starting mixture was added to a graphite capsule, which was in turn placed in a silica glass tube, evacuated and sealed with a torch, thus buffering the fO_2 at C–CO (~2–3 log units below IW). The sealed silica tube was placed inside the furnace adjacent to the thermocouple. Experiments run at temperatures below the Fe–C eutectic (975–1150 °C) were initially brought to a temperature of 1200 °C and held for 1 h before being lowered to the final run temperature and held for a period of 114–1512 h. The run times were chosen to allow time for diffusive equilibration between the solid metal and liquid (or troilite). Because diffusion in γ-Fe (Watson and Watson, 2003) is much slower than in S-rich liquids (Dobson, 2002) or troilite (Condit et al., 1974), diffusion through the solid metal was considered to be the rate-limiting step in exchange during these experiments. Based on diffusion data for several siderophile trace elements in solid Fe–Ni alloys (Watson and Watson, 2003), the run times were sufficient to allow the solid alloy to exchange trace elements with the liquid (or troilite) by diffusion over a distance of ~20–200 μm, comparable to the size of the solid alloy grains in these experiments.

The experiment at 1150 °C contained immiscible S-rich and C-rich liquids, rather than an S-rich liquid coexisting with solid γ-Fe. Experiments run at higher temperatures (1175–1350 °C), which also contained two immiscible liquids, were brought directly to the final run temperature and were held for a period of 4–384 h. The run times for the liquid/liquid partitioning experiments were sufficient to allow diffusive homogenization of the S-rich and C-rich liquid reservoirs, as diffusion in liquid iron and iron sulfides is several orders of magnitude faster than in solid γ-Fe (Dobson, 2000, 2002). A complete list of run conditions is given in Tables 1 and 2. At the conclusion of each run, the sealed silica tube was removed from the furnace and immediately quenched by submersion in cold water. The silica tubes were then opened, and the experimental charges were removed from the graphite capsules, mounted in epoxy, polished, and examined.

Back-scattered electron (BSE) images of some representative γ-Fe/S-rich liquid runs are shown in Fig. 1. The solid metal displays a texture indicative of a metastable Fe_3C phase that exsolves on quench. The S-rich liquid was a single phase at the run temperature, but quenched to a dendritic texture that is characteristic of rapidly cooled liquid sulfides. Relatively small areas of quenched sulfide liquid can be difficult to work with in that they may not yield representative bulk compositions; given the scale of the quench texture, we attempted to mitigate this by using either defocusing or rastering the beam during each analysis, and by performing separate analyses that sampled as much of the quenched liquid reservoir as possible. Fig. 2 shows representative BSE images of the experimental charges containing immiscible C-rich and S-rich liquids. The C-rich liquid coalesces in the center of the charge and is overlain by the sulfide liquid. There is quench texture present in both the C-rich and S-rich liquids.

Table 1
Phase compositions from solid/solid and solid/liquid partitioning experiments.

Run #	S16	S6	S4	S5	S7
Temperature (°C)	975	1025	1050	1100	1125
Duration (h)	1512	552	473	260	312
Bulk (wt%)					
Fe	75.14	75.14	75.14	75.14	75.14
S	24.25	24.25	24.25	24.25	24.25
Trace	0.61	0.61	0.61	0.61	0.61
γ-Fe metal					
Fe (wt%)	96.95 ± .24	97.77 ± .19	97.80 ± .23	97.71 ± .19	97.69 ± .31
S (wt%)	.006 ± .004	0.01 ± .01	0.01 ± .01	0.01 ± .01	0.02 ± .01
C (wt%)	1.51 ± .71	1.23 ± .72	1.35 ± .73	1.29 ± .73	1.51 ± .71
Trace (wt%)	0.51	0.55	0.58	0.76	0.69
Total (wt%)	98.98	99.56	99.58	99.77	99.91
Ag (ppm)	<1.2	1.84 ± 0.68	3.2 ± 0.2	5 ± 0.5	6 ± 5
As (ppm)	442 ± 85	449 ± 15	438 ± 36	448 ± 18	426 ± 13
Au (ppm)	620 ± 63	399 ± 4	348 ± 38	986 ± 33	349 ± 14
Co (ppm)	436 ± 24	346 ± 7	428 ± 35	449 ± 11	400 ± 11
Cr (ppm)	<28	28 ± 1	55 ± 6	54 ± 3	276 ± 9
Cu (ppm)	752 ± 24	199 ± 3	265 ± 29	232 ± 17	244 ± 12
Ge (ppm)	364 ± 10	392 ± 6	429 ± 25	421 ± 13	444 ± 8
Ir (ppm)	172 ± 41	520 ± 130	800 ± 240	1140 ± 240	890 ± 150
Mn (ppm)	<6	3.8 ± 2.8	6.5 ± 0.3	10.3 ± 0.8	18 ± 10
Mo (ppm)	514 ± 24	560 ± 18	571 ± 40	596 ± 13	596 ± 21
Ni (ppm)	441 ± 82	516 ± 8	419 ± 44	729 ± 16	560 ± 38
Os (ppm)	101 ± 67	362 ± 82	311 ± 95	394 ± 50	479 ± 75
Pd (ppm)	412 ± 32	399 ± 7	296 ± 16	390 ± 10	393 ± 9
Pt (ppm)	89 ± 56	448 ± 72	500 ± 110	416 ± 38	569 ± 147
Re (ppm)	200 ± 120	280 ± 110	280 ± 100	550 ± 170	580 ± 120
Ru (ppm)	245 ± 73	260 ± 16	295 ± 26	351 ± 36	339 ± 13
Se (ppm)	<42	<8	<10	<8	<6
W (ppm)	309 ± 45	307 ± 15	379 ± 12	419 ± 7	375 ± 16
Sulfide liquid (troilite)					
Fe (wt%)	61.61 ± .27	65.39 ± .21	65.94 ± .19	67.06 ± .28	66.69 ± .25
S (wt%)	37.87 ± .96	32.50 ± .78	31.88 ± .91	31.51 ± .96	32.00 ± .60
C (wt%)	nd	.075 ± .027	.086 ± .029	.081 ± .029	.082 ± .028
Trace (wt%)	0.72	1.08	0.99	0.90	1.01
Total (wt%)	100.20	99.035	98.896	99.551	99.782
Ag (ppm)	<2	1910 ± 43	2090 ± 850	1670 ± 440	1260 ± 580
As (ppm)	<47	106 ± 98	103 ± 19	180 ± 36	230 ± 120
Au (ppm)	3.4 ± 0.8	59 ± 15	43 ± 9	199 ± 35	77 ± 34
Co (ppm)	31 ± 7	103 ± 42	114 ± 25	159 ± 29	148 ± 47
Cr (ppm)	3400 ± 1400	975 ± 70	560 ± 200	340 ± 170	1920 ± 250
Cu (ppm)	1270 ± 110	3500 ± 2600	3800 ± 600	3200 ± 600	3200 ± 1200
Ge (ppm)	<92	<12	12 ± 9	9 ± 7	10 ± 7
Ir (ppm)	<1.1	<0.59	0.74 ± 0.31	0.19 ± 0.14	0.48 ± 0.44
Mn (ppm)	1970 ± 580	2820 ± 270	1930 ± 320	1380 ± 470	1680 ± 150
Mo (ppm)	126 ± 12	84 ± 17	73 ± 7	87 ± 29	75 ± 19
Ni (ppm)	–	359 ± 4	407 ± 140	860 ± 70	612 ± 87
Os (ppm)	<0.29	<0.5	0.28 ± 0.10	0.49 ± 0.38	0.08 ± 0.07
Pd (ppm)	<5.1	123 ± 87	210 ± 45	406 ± 24	333 ± 63
Pt (ppm)	<1.9	<1.79	<2	0.49 ± 0.38	<1.8
Re (ppm)	<0.5	<0.15	0.21 ± 0.15	0.085 ± 0.075	<0.6
Ru (ppm)	<3.3	<3	2.2 ± 1.9	1.6 ± 1.1	4.0 ± 3.5
Se (ppm)	384 ± 55	730 ± 370	590 ± 180	537 ± 86	590 ± 180
W (ppm)	0.68 ± 0.12	0.63 ± 0.35	0.46 ± 0.22	0.27 ± 0.15	0.18 ± 0.17

nd = below detection limit.

Table 2
Phase compositions from liquid/liquid partitioning experiments.

Run #	S1	S8	S10	S11	S12	S13
Temperature (°C)	1150	1175	1200	1250	1300	1350
Duration (h)	114	384	16	4	18	5
Bulk (wt%)						
Fe	75.14	75.14	88.53	88.53	88.53	88.53
S	24.25	24.25	11.16	11.16	11.16	11.16
Trace	0.61	0.61	0.31	0.31	0.31	0.31
C-rich liquid						
Fe (wt%)	94.69 ± .42	94.12 ± .54	94.33 ± .62	94.37 ± .40	93.91 ± .52	93.88 ± .42
S (wt%)	0.82 ± .30	1.44 ± .30	1.55 ± .40	1.41 ± .30	1.06 ± .40	1.23 ± .50
C (wt%)	2.95 ± .71	2.98 ± .76	3.06 ± .69	3.01 ± .71	2.91 ± .75	3.11 ± .75
Trace (wt%)	1.27	0.62	0.38	0.34	0.26	0.34
Total (wt%)	99.73	99.16	99.40	99.23	98.14	98.56
Ag (ppm)	10 ± 7	3.6 ± 1.1	11 ± 1	12 ± 2	0.90 ± 0.15	3.7 ± 0.7
As (ppm)	606 ± 73	385 ± 48	149 ± 5	154 ± 6	173 ± 21	180 ± 12
Au (ppm)	4100 ± 1300	403 ± 20	219 ± 8	29 ± 1	7.3 ± 0.5	960 ± 40
Co (ppm)	560 ± 150	357 ± 10	183 ± 4	162 ± 4	175 ± 2	155 ± 7
Cr (ppm)	167 ± 66	307 ± 28	168 ± 10	65 ± 3	184 ± 4	46 ± 2
Cu (ppm)	254 ± 67	196 ± 38	165 ± 12	225 ± 14	149 ± 20	157 ± 42
Ge (ppm)	580 ± 200	406 ± 26	168 ± 5	131 ± 5	151 ± 2	132 ± 7
Ir (ppm)	1080 ± 120	771 ± 40	480 ± 5	413 ± 10	285 ± 10	275 ± 3
Mn (ppm)	20 ± 13	23 ± 8	28 ± 3	38 ± 15	16 ± 2	12 ± 1
Mo (ppm)	760 ± 240	522 ± 46	345 ± 6	375 ± 25	232 ± 12	280 ± 26
Ni (ppm)	860 ± 290	541 ± 14	343 ± 15	341 ± 11	282 ± 5	255 ± 2
Os (ppm)	700 ± 65	430 ± 18	348 ± 5	347 ± 10	288 ± 50	192 ± 5
Pd (ppm)	690 ± 110	368 ± 20	348 ± 9	263 ± 7	159 ± 2	175 ± 14
Pt (ppm)	809 ± 69	509 ± 26	329 ± 6	356 ± 8	92 ± 8	128 ± 8
Re (ppm)	608 ± 65	407 ± 22	188 ± 8	214 ± 9	168 ± 6	187 ± 2
Ru (ppm)	340 ± 49	252 ± 18	145 ± 2	144 ± 6	120 ± 3	118 ± 2
Se (ppm)	<46	<19	8 ± 6	8 ± 6	<7	<7
W (ppm)	567 ± 22	325 ± 12	160 ± 3	152 ± 3	160 ± 6	133 ± 8
Sulfide liquid						
Fe (wt%)	68.33 ± .23	68.09 ± .31	68.47 ± .19	68.48 ± .33	68.31 ± .26	68.55 ± .20
S (wt%)	30.49 ± .72	30.71 ± .84	30.38 ± .76	30.56 ± .92	30.61 ± .76	30.43 ± .84
C (wt%)	0.197 ± .78	0.183 ± .88	0.185 ± .79	0.177 ± .81	0.181 ± .78	0.179 ± .79
Trace (wt%)	1.08	0.74	0.80	0.83	0.46	0.64
Total (wt%)	100.727	99.723	99.835	100.047	99.561	99.799
Ag (ppm)	980 ± 250	258 ± 68	930 ± 150	980 ± 160	114 ± 3	810 ± 200
As (ppm)	125 ± 32	132 ± 46	33 ± 5	40 ± 5	24 ± 5	41 ± 5
Au (ppm)	1610 ± 230	181 ± 30	70 ± 4	14 ± 1	1.6 ± 0.4	404 ± 75
Co (ppm)	215 ± 23	169 ± 18	73 ± 4	74 ± 9	47 ± 4	69 ± 11
Cr (ppm)	691 ± 53	1250 ± 160	624 ± 63	263 ± 55	461 ± 61	182 ± 46
Cu (ppm)	2220 ± 240	1720 ± 250	1840 ± 110	2210 ± 210	1240 ± 90	1500 ± 260
Ge (ppm)	19 ± 9	19 ± 12	14 ± 11	14 ± 8	9 ± 7	13 ± 9
Ir (ppm)	3.54 ± 0.38	2.3 ± 0.7	0.74 ± 0.38	1.03 ± 0.45	1.09 ± 0.47	0.65 ± 0.51
Mn (ppm)	2570 ± 700	2040 ± 220	2740 ± 210	3130 ± 590	1680 ± 100	2090 ± 830
Mo (ppm)	29 ± 2	23 ± 6	11 ± 1	11 ± 2	7.4 ± 1.2	8 ± 2
Ni (ppm)	908 ± 95	630 ± 100	427 ± 12	422 ± 42	339 ± 24	315 ± 2
Os (ppm)	0.82 ± 0.14	0.32 ± 0.12	0.15 ± 0.08	0.16 ± 0.09	0.20 ± 0.11	0.13 ± 0.09
Pd (ppm)	723 ± 66	429 ± 42	402 ± 34	359 ± 50	188 ± 7	240 ± 21
Pt (ppm)	11.2 ± 1.2	12.5 ± 2.6	5.5 ± 1.7	8.4 ± 2.0	1.7 ± 0.9	3.1 ± 1.8
Re (ppm)	0.56 ± 0.19	0.19 ± 0.16	<0.45	0.09 ± 0.08	0.17 ± 0.13	0.34 ± 0.21
Ru (ppm)	6 ± 2	5 ± 4	<7	2.2 ± 1.7	1.5 ± 1.1	1.5 ± 1.2
Se (ppm)	650 ± 130	510 ± 110	820 ± 30	790 ± 80	480 ± 30	680 ± 250
W (ppm)	1.4 ± 0.3	0.71 ± 0.26	0.33 ± 0.21	0.25 ± 0.20	0.25 ± 0.20	0.29 ± 0.24

2.1. Major element analyses

Each experiment was imaged and analyzed to determine major element compositions (Fe, S) using the Cameca SX-100 electron microprobe at the University of Michigan. The electron microprobe analyses were performed using beam conditions of 15 kV, 20 nA, counting times of 20 s and either a defocused 20 μm beam or a beam rastered over

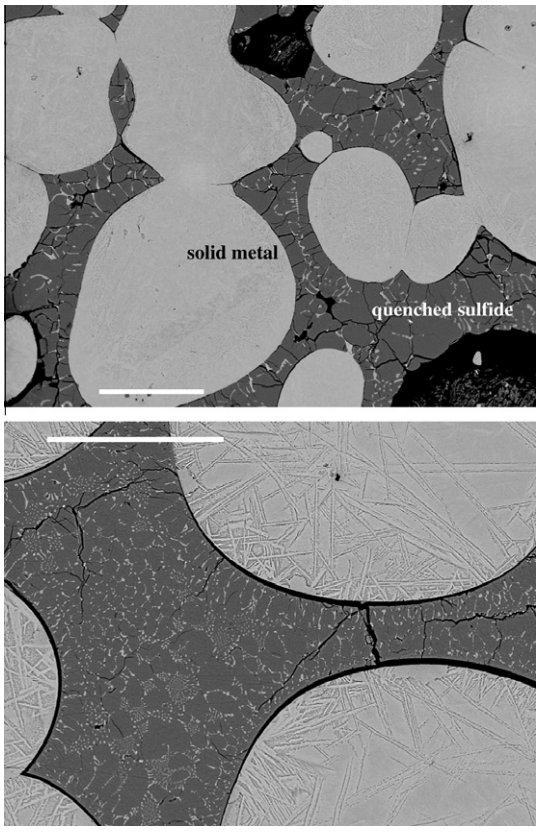

Fig. 1. A back-scattered electron (BSE) image of run #S-6 (1025 °C) (top) and #S-7 (1125 °C). Large grains of Fe-metal are surrounded by quenched sulfide melt. Scale bars are 100 μm.

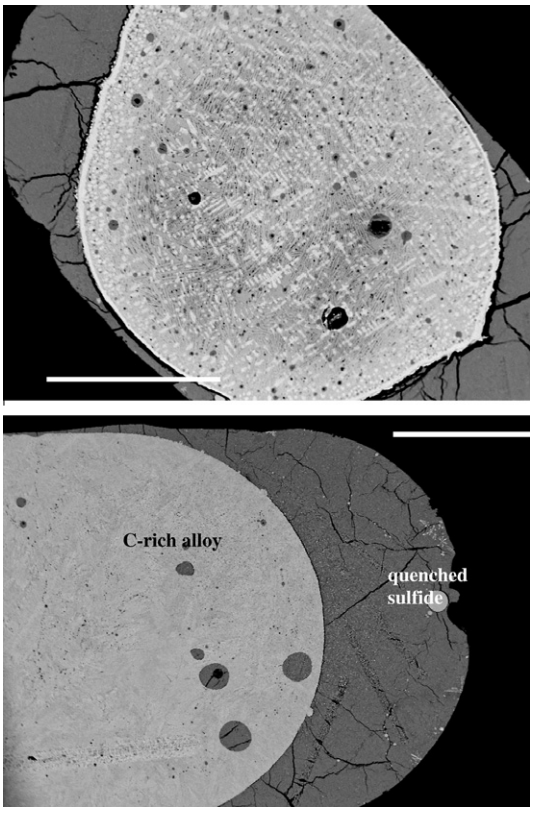

Fig. 2. A BSE image of run #S-1 (1150 °C) and #S-11 (1250 °C). The C-rich melt is in the center of the sample and is surrounded by quenched S-rich liquid. The C-rich liquid also displays a quench texture. Although the phases are generally well separated, melt inclusions are visible in both phases. Scale bars are 500 μm.

a 25 μm by 25 μm area. For each phase, 6–20 measurements were made and averaged to determine the bulk composition. Two approaches were used to perform the carbon analyses. One technique utilized an Al coating on the samples and standards, which in this case were an iron carbide as well as a piece of pure iron, which served as a carbon-free 'blank'. Following calibration, the blank was analyzed and any measured C was taken as the background level for subsequent analyses. The second technique involved analyses of uncoated surfaces; since the standards, samples, and blank are all metallic, a conductive carbon paint was used around the specimens to prevent charging, and the same protocol as the Al-coated technique was used. Both techniques yielded results that were in agreement within 5–10% of the other. The measured sulfur and carbon contents of the C-rich and S-rich liquids from the high-temperature experiments are in good agreement with the data of Wang et al. (1991), who used combustion analyses to determine S and C contents in immiscible liquids in the Fe–S–C system. The measured carbon concentrations in solid iron are also in agreement with existing data at graphite saturation (Okamoto, 1992).

2.2. Trace element concentrations

The trace element composition of each of the quenched phases in each experiment was analyzed by laser ablation inductively coupled plasma mass spectrometry (LA-ICP-MS) at the University of Maryland. In situ analyses were performed using a single-collector ThermoFinnigan Element 2 sector field ICP-MS coupled to a New Wave UP213UV laser ablation system. Ablation analyses were done in spot mode for the solid metal phase using an 80 μm beam diameter and a 6–7 Hz flash rate. Analyses were done in line scan mode for the metal and sulfide liquid phases using a 25–30 μm beam diameter and a 5–6 Hz flash rate, and were generally 300–1200 μm in length. Four to five spot analyses or line scans were performed on each phase per experiment. Data were collected for the following masses: ^{53}Cr, ^{55}Mn, ^{57}Fe, ^{59}Co, ^{62}Ni, ^{63}Cu, ^{74}Ge, ^{75}As, ^{77}Se, ^{95}Mo, ^{100}Ru, ^{105}Pd, ^{107}Ag, ^{109}Ag, ^{183}W, ^{184}W, ^{185}Re, ^{188}Os, ^{189}Os, ^{191}Ir, ^{193}Ir, ^{194}Pt, ^{195}Pt, and ^{197}Au. Analyses of run products were accompanied by four analyses performed on each of the three standard materials. These standard materials were NIST 610, JB sulfide, and the meteorite Hoba. These were analyzed before and after the run products in order to constrain the instrument drift. Electron microprobe analyses of Fe were used as an internal standard for these experiments, i.e., the Fe content determined by EPMA was compared to the ICP-MS count rate, and the concentrations of the trace elements were determined by the proportion of trace element count rates to the standard (Fe)

count rates. Table 1 provides the complete compositional information for solid/solid and solid/liquid runs and Table 2 provides the compositions of the phases in the immiscible liquid runs. Reported errors are twice the standard deviation of the weighted mean of the individual measurements. Measurements below the detection limit are indicated as limiting values.

3. RESULTS

The partition coefficient (D) for an element i between two coexisting phases is defined as:

$$D_i = \frac{C_i^1}{C_i^2}, \quad (1)$$

where C_i^1 is the concentration (in wt%) of element i in either the solid metal or C-rich liquid and C_i^2 is the concentration in either the S-rich liquid or troilite. Partition coefficients determined from each experiment, for the complete suite of elements studied, are reported in Table 3. If the measurement for an element in one of the phases was below the detection limit (as indicated in Table 1), a minimum or maximum D value was calculated and is indicated as such in Table 3. The partitioning results for each trace element are plotted as a function of temperature in Fig. 3, with solid/liquid data in the center of the temperature scale (1025–1125 °C; black circles).

3.1. Partitioning between solid metal and liquid sulfide

In general, temperature is considered to have a small direct influence on trace element partitioning in metallic systems (Jones and Malvin, 1990). The major influence of temperature is indirect, resulting from the control of temperature on the phase compositions, which in turn strongly influence the partition coefficients (Jones and Malvin, 1990; Jones et al., 1993; Chabot and Jones, 2003). In general, the concentration of non-metallic elements in the liquid is considered to be the primary control on trace element partitioning (Jones and Malvin, 1990; Chabot and Jones, 2003). In the present solid-metal/liquid-sulfide experiments, the major element composition of the liquid does not vary measurably with increasing temperature (Table 1 and Fig. 4), and hence we would expect to see little variation in the partition coefficients with temperature. This is true for many elements, but not all. For Ag, Cr, Mn and W the partition coefficient increases with temperature, while for Ni, Pd, and possibly As, Au and Ru the partition coefficient decreases with temperature (Fig. 3). No firm conclusions can be drawn about what controls these variations in the partition coefficients, but we offer the tentative suggestion that they are due to the influence of carbon dissolved in the solid. The concentration of carbon in solid Fe increases by 25% (from 7 to 8.7 at%) between 1025 and 1125 °C (Okamoto, 1992; our electron microprobe measurements are consistent with this but insufficiently precise to demonstrate it). The elements whose partition coefficients decrease with temperature (Ni, Pd, As, Au, Ru) have all been shown to have repulsive interactions with carbon in liquid Fe (Chabot et al., 2006). A similar repulsive interaction with carbon in solid Fe could explain the decrease in partition coefficient with temperature in our experiments. Of the elements whose partition coefficient decreases with temperature, Cr and W have been shown to have attractive interactions with carbon in liquid Fe (Chabot et al., 2006) and no data are available for Ag and Mn. An attractive interaction between these elements and carbon in solid Fe could explain the increase in partition coefficients with increasing temperature in this study.

A comparison of our data with partitioning data from the Fe–S system also suggests that carbon dissolved in solid Fe has a significant influence on trace element partitioning. Fig. 5 shows a comparison of the solid/liquid partition coefficients from our graphite-saturated experiments with partition coefficients from the pure Fe–S system, calculated at a similar liquid sulfur concentration (~31 wt% S, compared to ~32 wt% for our graphite-saturated experiments) using the parameterization of Chabot and Jones (2003). The primary difference between the Fe–S and Fe–S–C systems represented in Fig. 5 is that the solid metal in the Fe–S–C system contains a significant amount of carbon (carbon is present only at trace levels in the liquid). Elements repelled by carbon in the solid would thus have smaller partition coefficients in the Fe–S–C system, and elements attracted to carbon would have larger partition coefficients in the Fe–S–C system. In general, the elements that have larger partition coefficients in the Fe–S–C system tend to be those that are "anthracophile" (attracted to carbon) in liquid iron, while those that have smaller partition coefficients in the Fe–S–C system tend to be repelled by carbon in liquid iron (Fig. 5). This suggests that trace element interactions with carbon in solid iron are broadly similar to their interactions in liquid iron.

3.2. Partitioning between immiscible liquids

Between 1125 and 1150 °C, solid γ-Fe metal is replaced by a C-rich, S-bearing liquid which is immiscible with the sulfide liquid. The C-rich liquid remains the primary host phase for C and also, in contrast to the solid metal, accommodates some sulfur. The transition from solid to liquid metal is indicated by a textural change in the samples (Fig. 2), the above-noted change in S concentration, and a distinct change in partitioning behavior for some of the trace elements. The liquid metal/liquid sulfide partition coefficients are listed in Table 3 and are plotted as a function of temperature in Fig. 3 (1150–1350 °C; black squares). The liquid compositions and liquid/liquid trace element partition coefficients remain nearly constant as temperature increases.

For most of the trace elements there is no drastic change in the partition coefficient at the transition to liquid immiscibility, but for some elements there are distinct changes in the partition behavior. It is useful to view these changes in terms of the ratio of the solid-metal/liquid-sulfide partition coefficient to the liquid-metal/liquid-sulfide partition coefficient; because the liquid sulfide has similar (although not identical) composition in the solid/liquid and liquid/liquid experiments, this ratio essentially gives the partition coefficient between C-rich solid metal and C-rich liquid metal,

Table 3
Trace element partition coefficients.

Run #	S16	S6	S4	S5	S7	S1	S8	S10	S11	S12	S13
Temperature (°C)	975	1025	1050	1100	1125	1150	1175	1200	1250	1300	1350
D(Ag)	–	0.001 ± .0004	0.0015 ± 0.0006	0.0030 ± 0.0008	0.0047 ± 0.0045	.010 ± .008	.014 ± .006	.012 ± .002	.013 ± .003	.008 ± .001	.005 ± .001
D(As)	>7.6	4.2 ± 2	4.3 ± 0.9	2.5 ± 0.5	1.8 ± 0.9	4.8 ± 1.4	2.9 ± 1.1	4.5 ± 0.7	3.9 ± 0.5	7.2 ± 1.7	4.4 ± 0.6
D(Au)	182 ± 46	6.8 ± 1.7	8.1 ± 1.9	5.0 ± 0.9	4.5 ± 2.0	2.5 ± 0.9	2.2 ± 0.4	3.1 ± 0.2	2.1 ± 0.2	4.5 ± 1.0	2.4 ± 0.4
D(Co)	14 ± 3	3.4 ± 1.4	3.8 ± 0.9	2.8 ± 0.5	2.7 ± 0.9	2.6 ± 0.8	2.1 ± 0.2	2.51 ± 0.15	2.2 ± 0.3	3.7 ± 0.3	2.2 ± 0.4
D(Cr)	<0.014	.029 ± .002	.099 ± .037	0.16 ± .08	0.14 ± 0.02	0.24 ± 0.10	0.25 ± 0.04	0.27 ± 0.03	0.25 ± 0.05	0.40 ± 0.05	0.25 ± 0.06
D(Cu)	0.59 ± .05	.056 ± .023	.070 ± .013	.072 ± .015	.077 ± .029	0.11 ± 0.03	0.11 ± 0.03	0.09 ± 0.01	0.10 ± 0.01	0.12 ± 0.02	0.10 ± 0.03
D(Ge)	>3.8	>32	36 ± 15	47 ± 20	44 ± 18	30 ± 14	21 ± 8	12 ± 5	9 ± 3	17 ± 7	10 ± 4
D(Ir)	>120	>670	1090 ± 460	6000 ± 3300	1900 ± 1000	300 ± 50	330 ± 80	650 ± 210	400 ± 120	260 ± 80	420 ± 180
D(Mn)	<0.0043	.0013 ± .0010	0.0034 ± 0.0006	0.0075 ± 0.0026	.011 ± .006	.008 ± .006	.011 ± .004	.010 ± .001	.012 ± .005	.010 ± .001	.006 ± .002
D(Mo)	4.1 ± 0.4	6.7 ± 1.4	7.8 ± 0.9	6.9 ± 2.3	7.9 ± 2.0	26 ± 9	23 ± 6	31 ± 3	34 ± 7	31 ± 5	35 ± 9
D(Ni)	–	1.44 ± 0.03	1.03 ± .37	0.85 ± 0.07	0.92 ± 0.14	0.95 ± 0.23	0.86 ± 0.14	0.80 ± 0.04	0.81 ± 0.08	0.83 ± 0.06	0.81 ± 0.01
D(Os)	>117	>560	1110 ± 450	900 ± 300	6000 ± 3200	900 ± 200	1300 ± 400	2300 ± 800	2200 ± 800	1400 ± 700	1500 ± 600
D(Pd)	>75	3.2 ± 1.3	1.4 ± 0.3	0.96 ± 0.06	1.2 ± 0.2	0.96 ± 0.18	0.86 ± 0.10	0.87 ± 0.08	0.73 ± 0.10	0.85 ± 0.03	0.73 ± 0.09
D(Pt)	>17	>210	>196	850 ± 390	>290	72 ± 10	41 ± 8	60 ± 14	42 ± 8	53 ± 20	41 ± 16
D(Re)	>154	>1170	1340 ± 720	6500 ± 3500	>765	1090 ± 350	2140 ± 980	>400	2400 ± 1100	990 ± 420	550 ± 200
D(Ru)	>52	>81	140 ± 70	220 ± 100	90 ± 40	57 ± 21	50 ± 23	>21	65 ± 28	80 ± 33	79 ± 34
D(Se)	<0.13	<0.022	<0.024	<0.018	<0.015	<0.09	<0.05	.010 ± .007	.010 ± .008	<0.015	<0.016
D(W)	450 ± 100	490 ± 180	820 ± 260	1550 ± 540	2080 ± 990	400 ± 80	460 ± 120	480 ± 180	610 ± 260	640 ± 280	460 ± 210

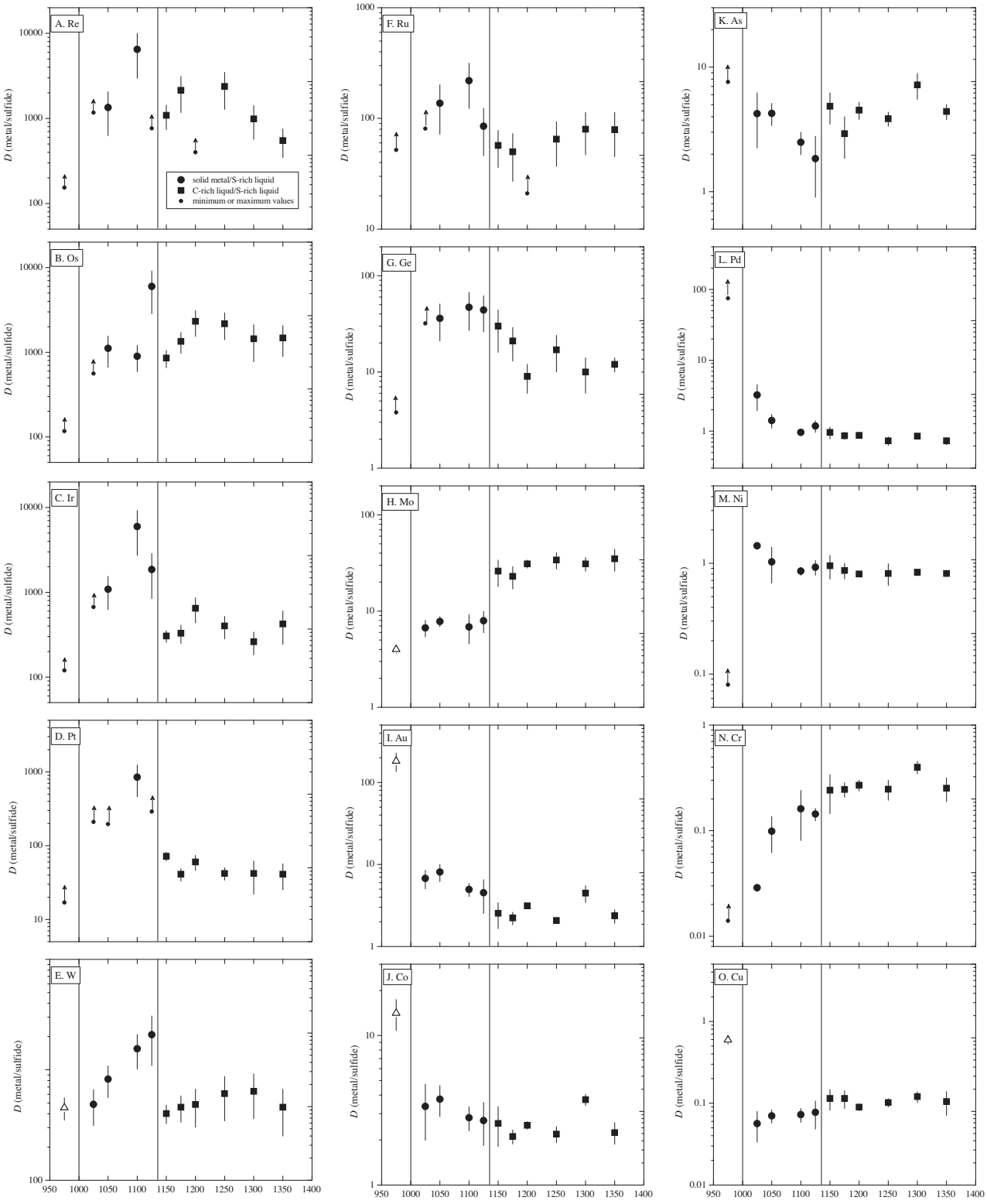

Fig. 3. The solid/solid (open triangles), solid/liquid (solid circles) and liquid/liquid (solid squares) partition coefficients (D) for (A) Re, (B) Os, (C) Ir, (D) Pt, (E) E, (F) Ru, (G) Ge, (H) Mo, (I) Au, (J) Co, (K) As, (L) Pd, (M) Ni, (N) Cr, (O) Cu, (P) Mn, (Q) Ag, (R) Se and (S) Fe are plotted as a function of temperature. Small solid circles with arrows represent minimum values of D. Error bars show 2σ uncertainties in the partition coefficients.

and it can be compared to the solid/liquid partition coefficient in the Fe–C system. This comparison is shown in Fig. 6. In general the solid-metal/C-rich liquid partition coefficients calculated from our experimental data are in

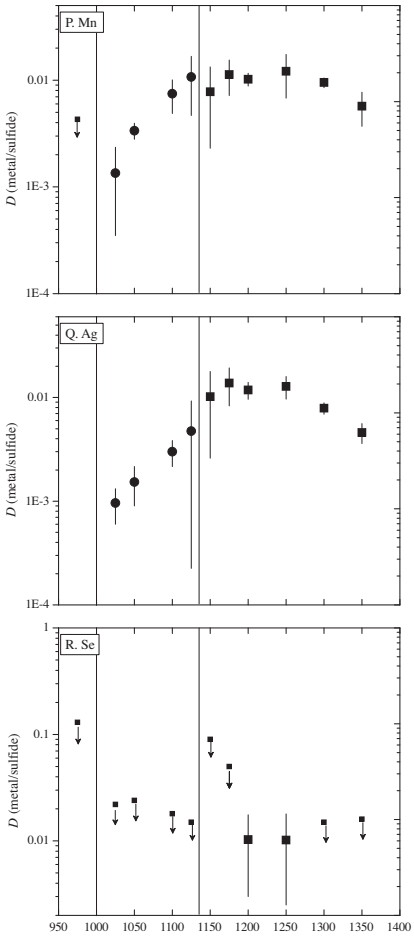

Fig. 3. *(continued)*

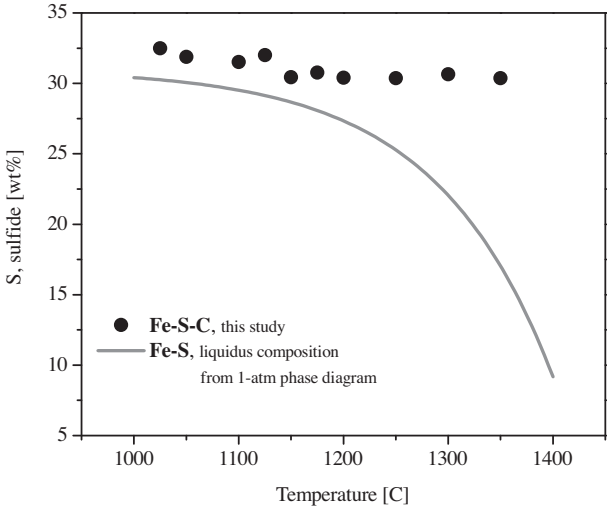

Fig. 4. A comparison of the S content of S-rich liquid as a function of temperature in the binary Fe–S system vs. the ternary Fe–S–C system. In the Fe–S–C system, the presence of C keeps the S content of the S-rich liquid nearly constant, and much higher than in the Fe–S system at higher temperatures.

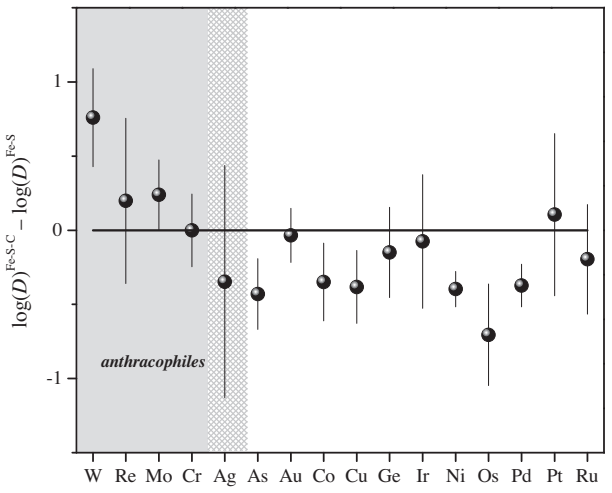

Fig. 5. Difference in solid/liquid partition coefficients between the Fe–S–C system from this study (average of 1100 and 1125 °C experiments) and the pure Fe–S system at similar S concentration in the liquid (31 wt%).

reasonable agreement with the measured values in the Fe–C system, and most of the discrepancies can be explained by the presence of sulfur in our experiments. In general, our values tend to be larger than those in the Fe–C system for siderophile elements and smaller for chalcophile elements. This trend can be explained by the presence of sulfur in the C-rich liquid in our experiments, which increases the partition coefficient for elements that have repulsive interactions with sulfur (siderophiles) and reduces it for elements that are attracted to sulfur (chalcophiles).

An important result of adding carbon to the Fe–S system is that the partition coefficients for many elements, particularly the highly siderophiles (HSE), remain large to much higher temperatures. At 1350 °C, in the Fe–FeS system the S concentration in the liquid is ~15 wt%, and the solid/liquid D values at this S concentration are ~10 or less for all elements (Chabot and Jones, 2003). In contrast, the liquid/liquid D values in the graphite-saturated system at the same temperature are on the order of 1000 for elements such as Re, Os and Ir (Fig. 7). These large partition coefficients are due to the presence of carbon, which keeps the S concentration in the sulfide liquid high (~30 wt%) and causes elements that are strongly repelled by S to be sequestered in the C-rich liquid. The partition coefficients are expected to remain similarly high to even higher temperatures, because the miscibility gap remains large (and even widens slightly) up to temperatures of at least 1600 °C, at atmospheric pressure (Wang et al., 1991). This implies that in small planetary bodies that contain substantial abundances of both carbon and sulfur, highly siderophile elements will be strongly fractionated between immiscible S-rich and C-rich liquids over a broad range of temperatures. The ureilite parent body is probably one such body, and the siderophile element abundances in ureilites are discussed below in light of the present liquid/liquid and solid/liquid partitioning data.

The miscibility gap between C-rich and S-rich liquids becomes smaller at higher pressures, and closes entirely at

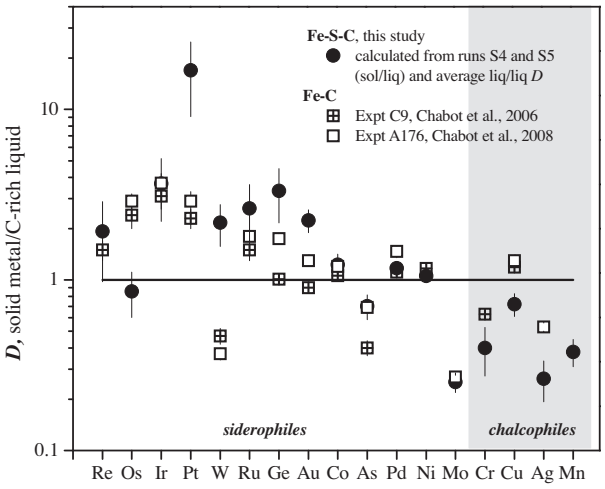

Fig. 6. Comparison of solid metal/C-rich liquid partition coefficients. Black circles represent the Fe–S–C system, and were calculated from the average of the solid metal/S-rich liquid D values from the 1050 and 1100 °C experiments, and the average of all values for C-rich liquid/S-rich liquid experiments. Open squares represent the Fe–C system at 5 GPa (Chabot et al., 2008) and crossed squares represent the Fe–C system at 1 atm (Chabot et al., 2006). The Fe–C data points were selected because the C contents of the C-rich liquid and C-rich solid most closely matches that of our experiments.

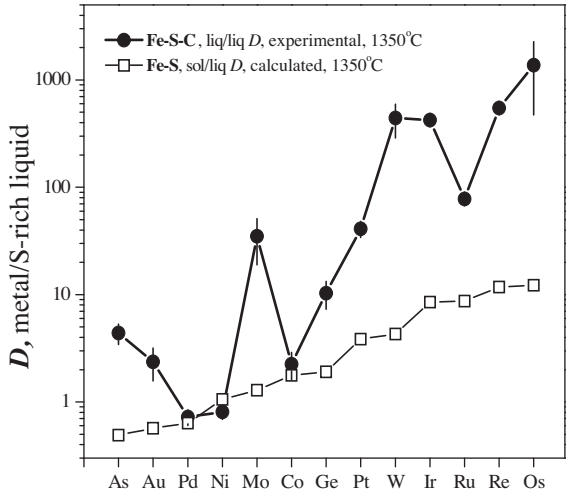

Fig. 7. Comparison of partition coefficients between immiscible liquids in the Fe–S–C system (solid circles), and solid metal/sulfide in the Fe–S system (open squares) at 1350 °C. The addition of carbon to the Fe–S system keeps the S concentration of the S-rich liquid high, supporting large D values for the highly siderophile elements (~10–100 times higher than in the Fe–S system).

~5–6 GPa (Corgne et al., 2008; Dasgupta et al., 2009). Because the compositions of C-rich and S-rich immiscible liquids become closer to each other at higher pressures, trace elements may be expected to be less strongly fractionated between the two liquids in larger planetary bodies. However, the interactions between trace elements and non-metals can change at high pressure (Chabot et al., 2011) and the behavior of trace elements in Fe–S–C immiscible liquids at high pressures therefore needs to be investigated experimentally.

3.3. Solid-metal/troilite partitioning

A single experiment was run at 975 °C, below the solidus in the Fe–S–C system. At this temperature, the two phases coexisting with graphite are C-bearing Fe metal and troilite, FeS. The solid-metal/troilite partitioning data are listed in Table 3, and shown in Fig. 3. Unfortunately, most of our data are lower or upper limits because the concentration was below the detection limit in either troilite or metal. Few data on trace element partitioning between troilite and metal exist in the literature, but in one case (Mo) we can compare our value for the graphite-saturated system to the value determined in the Fe–S system (Jones et al., 1993). Our value is a factor of ~3 higher (4.1 vs. 1.4), which again suggests that Mo is anthracophile in solid metal as well as in liquid metal (Chabot et al., 2008).

4. IMPLICATIONS FOR UREILITES

Ureilites are ultramafic achondrites that are considered to be residues of partial melting within the mantle of a carbon-rich asteroid (Goodrich, 1992; Middlefehldt et al., 1998). Despite having experienced high temperatures (up to ~1300 °C) and relatively high degrees of partial melting (~20–30%), ureilites retain a significant amount of iron metal and relatively high abundances of siderophile elements. Investigations of the siderophile abundance patterns in ureilites have noted a correlation with solid metal/liquid metal partition coefficients in the Fe–S system, suggesting that the parent body experienced partial loss of a sulfur-rich metallic liquid (Janssens et al., 1987; Goodrich et al., 1987; Humayun et al., 2005; Warren et al., 2006; Rankenburg et al., 2008). Ureilites thus appear to record an early stage of planetary differentiation, which included substantial igneous processing but only partial differentiation of a metallic core.

Heating of ureilites continued up to ~1300 °C, significantly higher than the Fe–S eutectic (988 °C) or the Fe–C eutectic (1153 °C). However, few studies have considered the effects of this high-temperature stage on siderophile element fractionation. Rankenburg et al. (2008) and Van Orman et al. (2009) examined siderophile element fractionation under the assumption that melting in the Fe–S system dominated the behavior at low temperatures and melting in the Fe–C system dominated at higher temperatures. However, one of the critical assumptions behind this modeling is that most of the S originally present was lost in the form of liquid during the low-T phase (thus, the high T phase could be approximated as pure Fe–C). In fact, this assumption may be wrong. Sulfur-rich liquids could potentially have been extracted from the mantle of the ureilite parent body (UPB) over a broad range of temperatures, beginning at the solidus of the Fe–S–C system (between ~975 and 988 °C at graphite saturation) and extending well into the field of liquid immiscibility at higher temperatures.

Experimental data on the permeability of silicate matrices to S-rich liquids indicate that extraction is favored under high temperatures, after a significant amount of melting of the silicates has already taken place (Bagdassarov et al., 2009). Considering this, the extraction of S-rich liquids from ureilites may be expected to occur mostly at high temperatures, in the field of liquid immiscibility. The fractionation of siderophile trace elements in C-rich liquid/S-rich liquid systems has not been considered previously due to the lack of data. By examining whether the solid/liquid or liquid/liquid partition coefficients are better able to model the siderophile element data from ureilites, it may be possible to distinguish whether the extraction of S-rich liquids from the ureilite mantle occurred primarily at temperatures below or above the transition to liquid immiscibility. This in turn could provide important information on the early differentiation of planetesimals in general. The elements W, Pt, Mo and Ge have significantly different partitioning behavior between solid/liquid and liquid/liquid systems, and these elements may be especially useful in identifying the conditions of S-rich liquid extraction.

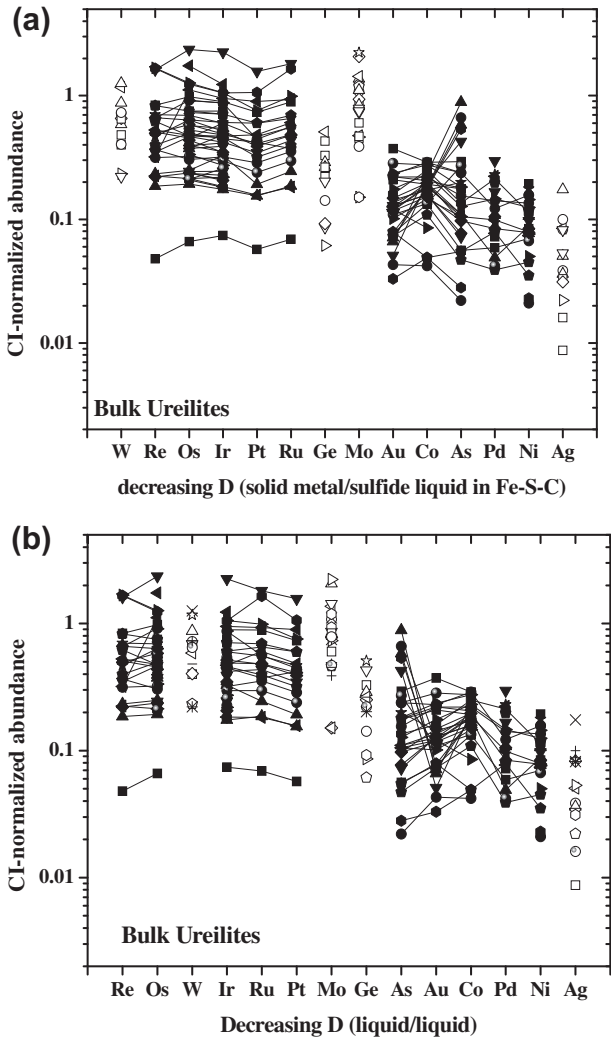

Fig. 8. Plots of CI-normalized abundances of siderophile elements in bulk ureilites. (a) Elements arranged in order of decreasing partition coefficient for solid metal vs. S-rich liquid in Fe–S–C system. (b) Elements arranged in order of decreasing partition coefficient for C-rich liquid vs. S-rich liquid in the Fe–S–C system. Note that relative Mo and Ge values of bulk ureilites are more consistent with liquid/liquid rather than solid/liquid fractionation. Data shown with filled symbols and lines are combined data for 43 ureilites from Rankenburg et al. (2008). Warren and Kallemeyn (1992), Kallemeyn and Warren (1994) and Warren et al. (2006). Multiple analyses of same meteorite have been averaged. All data for W, Mo, Ge and Ag are from other sources: W data are from Lee et al. (2009) and Spitz (1992); Mo data are from Spitz (1992); Ge data are from Wasson et al. (1976) and Higuchi et al. (1976).

Fig. 8 shows selected CI-chondrite normalized siderophile element concentrations for bulk ureilites plotted against the partition coefficients from this study for solid γ-Fe/S-rich liquid (Fig. 8a) and C-rich liquid/S-rich liquid (Fig. 8b). An important problem in making this comparison is the lack of datasets that include all relevant siderophile elements. We have shown one combined dataset (solid symbols and line) for Re, Os, Ir, Ru, Pt, As, Au, Co, Pd and Ni, for 43 ureilites, from several recent studies that appear to be consistent with one another (Rankenburg et al., 2008; Warren and Kallemeyn, 1992; Kallemeyn and Warren, 1994; Warren et al., 2006). Unfortunately, all available data for W, Mo and Ge are from other sources: the W data are from Lee et al. (2009) and Spitz (1992); the Mo data are from Spitz (1992) and the Ge data are from Wasson et al. (1976) and Higuchi et al. (1976). Despite the significant uncertainties introduced by having to mix these datasets (in particular, the possibility that different amounts of metal have been sampled in the analyzed aliquots), some clear patterns emerge in Fig. 8. Elements that are highly compatible in the solid metal or the C-rich liquid, with $D > 10$, have similarly high chondrite-normalized concentrations, while those that are less compatible are relatively depleted. This trend is consistent with the loss of a sulfur-rich liquid that takes with it a substantial fraction of the incompatible and moderately compatible siderophile elements. For the more commonly measured, and more compatible elements (including Pt and W), it would be difficult to distinguish the fit in Fig. 8a (liquid/liquid fractionation) from that in Fig. 8b (solid/liquid fractionation). However, for Mo and Ge the fit is much better for liquid/liquid fractionation. The solid/liquid partition coefficient for Mo is similar to those for Au, As and Co, yet these elements are depleted in ureilites compared to the highly siderophile elements, while Mo is not. If S-rich liquid were lost at low temperatures, in the presence of solid metal, one would expect Mo to be depleted in the residue similarly to Au, As and Co. The liquid/liquid partition coefficient for Mo is significantly larger than the solid/liquid partition coefficient, placing it more in line with the highly siderophile elements (Fig. 8b).

The element ratio Mo/Ge in particular should be a useful indicator of the conditions of metal extraction. In solid-Fe/S-rich liquid partitioning, $D_{Ge} > D_{Mo}$ by a factor of ~3, while $D_{Mo} > D_{Ge}$ by about the same factor in C-rich liquid/S-rich liquid partitioning. These two elements also have partition coefficients that are in the right range

(~5–50) to make them sensitive to S-rich liquid extraction processes; elements with much larger partition coefficients are quantitatively retained in the solid or C-rich liquid, while elements with much smaller partition coefficients are quantitatively transferred to the S-rich liquid. One potential problem with this element pair is that Ge has relatively high volatility (e.g., Wasson and Wai, 1976), and hence may have been lost from the ureilite parent body in a gas phase rather than solely by the loss of S-rich metallic liquid. With this caveat, and the important caveat noted above that Mo and Ge analyses are from different studies, the available data for Mo and Ge indicate that Mo/Ge in bulk ureilites is >1 (Fig. 8) – suggesting that S-rich liquids are extracted at high temperatures where an immiscible C-rich liquid is present, rather than at low temperatures in the presence of solid metal.

As with Mo and Ge, the partitioning behavior of Pt also undergoes an abrupt change as the temperature rises into the field of liquid immiscibility, with D_{Pt} decreasing by a factor of ~10. In the liquid/liquid system, the partition coefficient for Pt is similar to that for Ru, whereas in the solid/liquid system D_{Pt} is about an order of magnitude larger than D_{Ru}. To address how element ratios involving Pt vary between the solid/liquid and liquid/liquid cases, we have employed a batch melting model where the concentration in the solid or C-rich liquid, C_s, is given by:

$$\frac{C_5}{C_5^0} = \frac{D}{F(1-D)+D}. \quad (2)$$

In this equation, C_s^0 is the initial bulk concentration of the element of interest, which is taken to be chondritic, D is the solid/liquid or C-rich liquid/S-rich liquid partition coefficient and F is the proportion of S-rich liquid, which can take values between 0 and 1. Since the D values for the elements of interest do not exhibit strong trends with temperature, the average D values for solid/liquid and liquid/liquid, respectively, were used in the modeling. A batch extraction model was used instead of a fractional extraction model, because in a fractional model all S-rich liquid is removed as soon as it is produced. Therefore, in a fractional melting scenario, immiscible S-rich and C-rich liquids would never form, because all S would be removed from the system at the eutectic temperature (e.g., Van Orman et al., 2009).

Fig. 9 shows a plot of Pt/Ru vs. Pt/Os in the residual C-rich metal (solid or liquid) after different proportions of S-rich liquid metal have been removed. The heavy black line is the trend for liquid/liquid partitioning and the light gray line is the trend for solid/liquid partitioning; hash marks indicate the S-rich liquid fraction F and open circles show bulk concentration ratio data from ureilites (Rankenburg et al., 2008). Concentration ratios of Pt/Ru and Pt/Os in the residual metal follow two distinctly different paths due to the sharp decrease in D_{Pt} at the transition from solid/liquid to liquid/liquid. In both the solid/liquid and liquid/liquid systems $D_{Pt} < D_{Os}$, and therefore in both cases the ratio Pt/Os in the residual metal decreases as the proportion of S-rich liquid (F) increases. However, the Pt/Ru ratio behaves differently in the solid/liquid and liquid/liquid systems. In the solid/liquid system $D_{Pt} > D_{Ru}$, and the Pt/Ru ratio increases as F increases, whereas in the liquid/liquid system $D_{Pt} \approx D_{Ru}$ (the average value for Pt is slightly smaller), and there is little change in the Pt/Ru ratio with increasing F. As with the available Mo/Ge data, the internally consistent Rankenburg et al. (2008) data for ureilites are more consistent with S-rich liquid extraction from an immiscible liquid system above 1125 °C, rather than from residual solid metal at lower temperatures.

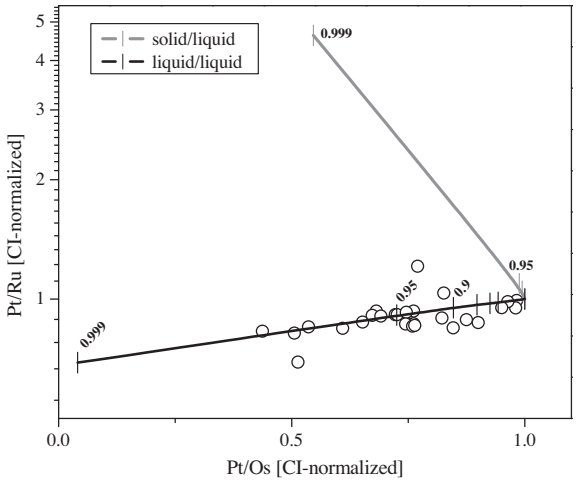

Fig. 9. A plot of batch extraction model calculations and ureilite data for Pt/Ru vs. Pt/Os (CI-chondrite normalized). Lines show model concentration ratios in residual solid (gray line) and residual C-rich liquid (heavy black line) after S-rich liquid extraction, with hash marks representing the fraction (F) of S-rich liquid removed from the system in increments of 0.05. Open circles are ureilite data from Rankenburg et al. (2008). Extraction of S-rich liquid from an immiscible liquid system seems to provide a good fit to the ureilite data.

Preferential extraction of an S-rich liquid at temperatures above 1125 °C requires that the S-rich liquid is significantly more mobile in the silicate matrix than the C-rich liquid. To our knowledge there are no data on the permeability or wetting behavior of C-rich liquids in silicate matrices. Holzheid et al. (2000) have shown that the dihedral angle between metal and olivine decreases as the molar ratio of anions to cations in the metal increases. In the Fe–S–C system, the S-rich liquid has a much larger anion/cation ratio than the C-rich liquid (~0.8 vs. ~0.2), and on this basis one would predict a larger dihedral and lower mobility for the C-rich liquids. Experimental data on the mobility of C-rich liquids in silicate matrices are needed to test this prediction.

ACKNOWLEDGEMENTS

This work was supported by grants from NASA (NNX09AB93G) and NSF (EAR0838141) to J.V.O. and NNX08AG63G to C.A.G. The authors wish to thank Carl Henderson for his assistance with electron microprobe analyses, and Anna Spitz for providing her dissertation data for ureilites. The authors wish to thank Nancy Chabot, Rajdeep Dasgupta and an anonymous reviewer for their constructive remarks.

REFERENCES

Bagdassarov N., Solferino G., Golabek G. J. and Schmidt M. W. (2009) Centrifuge assisted percolation of Fe–S melts in partially molten peridotite: time constraints for planetary core formation. *Earth Planet. Sci. Lett.* **288**, 84–95.

Brandon A. D. and Walker R. J. (2005) The debate over core–mantle interaction. *Earth Planet. Sci. Lett.* **232**, 211–225.

Chabot N. L., Campbell A. J., Jones J. H., Humayun M. and Agee C. B. (2003) An experimental test of Henry's Law in solid metal–liquid metal systems with implications for iron meteorites. *Met. Planet. Sci.* **38**, 181–196.

Chabot N. L., Campbell A. J., Jones J. H., Humayun M. and Lauer H. V. (2006) The influence of carbon on trace element partitioning behavior. *Geochim. Cosmochim. Acta* **70**, 1322–1335.

Chabot N. L., Campbell A. J., McDonough W. F., Draper D. S., Agee C. B., Humayan M., Watson H. C., Cottrell E. and Saslow S. A. (2008) The Fe–C system at 5 GPa and implications for Earth's core. *Geochim. Cosmochim. Acta* **72**, 4146–4158.

Chabot N. L. and Drake M. J. (2000) Crystallization of magmatic iron meteorites: the effects of phosphorus and liquid immiscibility. *Met. Planet. Sci.* **35**, 807–816.

Chabot N. L. and Jones J. H. (2003) The parameterization of solid metal–liquid metal partitioning of siderophile elements. *Met. Planet. Sci.* **38**, 1425–1436.

Chabot N. L., McDonough W. F., Jones J. H., Saslow S. A., Ash R. D., Draper D. S. and Agee C. B. (2011) Partitioning behavior at 9 GPa in the Fe–S system and implications for planetary evolution. *Earth Planet. Sci. Lett.* **305**, 425–434.

Condit R. H., Hobbins R. R. and Birchenall C. E. (1974) Self-diffusion of iron and sulfur in ferrous sulfide. *Oxid. Metals* **8**, 409–455.

Corgne A., Wood B. J. and Fei Y. (2008) C- and S-rich molten alloy immiscibility and core formation of planetesimals. *Geochim. Cosmochim. Acta* **72**, 2409–2416.

Corrigan C. M., Chabot N. L., McCoy T. J., McDonough W. F., Watson H. C., Saslow S. A. and Ash R. D. (2009) The iron–nickel–phosphorus system: effects on the distribution of trace elements during the evolution of iron meteorites. *Geochim. Cosmochim. Acta* **73**, 2674–2691.

Dobson D. P. (2000) ^{57}Fe and Co tracer diffusion in liquid Fe–FeS at 2 and 5 GPa. *Phys. Earth. Planet. Inter.* **120**, 137–144.

Dobson D. P. (2002) Self-diffusion in liquid Fe at high pressure. *Phys. Earth Planet. Inter.* **130**, 271–284.

Dasgupta R., Buono A., Whelan G. and Walker D. (2009) High-pressure melting relations in Fe–C–S systems: implications for formation, evolution, and structure of metallic cores in planetary bodies. *Geochim. Cosmochim. Acta* **73**, 6678–6691.

Fleet M. E., Liu M. and Crocket J. H. (1999) Partitioning of trace amounts of highly siderophile elements in the Fe–Ni–S system and their fractionation in nature. *Geochim. Cosmochim. Acta* **63**, 2611–2622.

Goodrich C. A. (1992) Ureilites: a critical review. *Meteoritics* **27**, 327–352.

Goodrich C. A., Jones J. H. and Berkley J. L. (1987) Origin and evolution of the ureilite parent magmas: multi-stage igneous activity on a large parent body. *Geochim. Cosmochim. Acta* **51**, 2255–2273.

Haack H. and Scott E. R. D. (1993) Chemical fractionations in Group IIIAB iron meteorites: origin by dendritic crystallization of an asteroidal core. *Geochim. Cosmochim. Acta* **571**, 3457–3472.

Higuchi H., Morgan J. W., Ganapathy R. and Anders E. (1976) Chemical fractionations in meteorites – X . Ureilites. *Geochim. Cosmochim. Acta* **40**, 1563–1571.

Holzheid A., Schmitz M. D. and Grove T. L. (2000) Textural equilibria of iron sulfide liquids in partly molten silicate aggregates and their relevance to core formation scenarios. *J. Geophys. Res.* **105**, 13555–13567.

Humayun M., Rushmer T., Rankenburg K. and Brandon A. D. (2005) A model for siderophile element distribution in planetary differentiation. *Lunar and Planetary Science Conference XXXVI,* 2208.

Janssens M.-J., Hertogen J., Wolf R., Ebihara M. and Anders E. (1987) Ureilites: trace element clues to their origin. *Geochim. Cosmochim. Acta* **51**, 2275–2283.

Jones J. H. and Malvin D. J. (1990) A nonmetal interaction model for the segregation of trace metals during solidification of Fe–Ni–S, Fe–Ni–P and Fe–Ni–S–P alloys. *Metall. Mat. Trans. B* **21B**, 697–706.

Jones J. H., Hart S. R. and Benjamin T. M. (1993) Experimental partitioning studies near the Fe–FeS eutectic, with an emphasis on elements important to iron meteorite chronologies (Pb, Ag, Pd and Tl). *Geochim. Cosmochim. Acta* **57**, 453–460.

Kallemeyn G. K. and Warren P. H. (1994) Geochemistry of LEW 88774 and two other unusual ureilites. *Lunar Planet. Sci.* **23**, 663–664.

Kelly W. R. and Larimer J. W. (1977) Chemical fractionations in meteorites—VIII. Iron meteorites and the cosmochemical history of the metal phase. *Geochim. Cosmochim. Acta* **41**, 93–111.

Lauer H. V., Jones J. H. and Schwandt C. S. (2001) Influence of carbon and sulfur on the partitioning of tungsten between solid and liquid metal. *Lunar and Planetary Science Conference XXXII*, 1948.

Lee D.-C., Halliday A. N., Singletary S. J. and Grove T. L. (2009) ^{182}Hf–^{182}W chronometry and early differentiation of the ureilite parent body. *Earth Planet. Sci. Lett.* **288**, 611–618.

Li J. and Agee C. B. (1996) Geochemistry of core–mantle differentiation at high pressure. *Nature* **381**, 686–689.

Li J. and Agee C. B. (2001) The effect of pressure, temperature, oxygen fugacity and composition on partitioning of nickel and cobalt between liquid Fe–Ni–S alloy and liquid silicate: implications for the Earth's core formation. *Geochim. Cosmochim. Acta* **65**, 1821–1832.

Li J., Fei Y., Mao H. K., Hirose K. and Shieh S. R. (2001) Sulfur in the Earth's inner core. *Earth Planet. Sci. Lett.* **193**, 509–514.

Liu M. and Fleet M. E. (2001) Partitioning of siderophile elements (W, Mo, As, Ag, Ge, Ga, and Sn) and Si in the Fe–S system and their fractionation in iron meteorites. *Geochim. Cosmochim. Acta* **65**, 671–682.

Middlefehldt D. W., McCoy T. J., Goodrich C. A. and Kracher A. (1998) Non-chondritic meteorites from asteroidal bodies. In *Reviews in Mineralogy and Geochemistry, vol. 36* (ed. P. H. Ribbe). Mineralogical Society of America, Washington, DC, pp. 4-73–4-95.

Okamoto H. (1992) The C–Fe (carbon–iron) system. *J. Phase Equilibria* **13**, 543–565.

Rankenburg K., Humayan M., Brandon A. D. and Herrin J. S. (2008) Highly siderophile elements in ureilites. *Geochim. Cosmochim. Acta* **72**, 4642–4659.

Spitz A. H. (1992) Trace element analysis of ureilite meteorites and implications for their petrogenesis. Ph. D. dissertation, University of Arizona.

Van Orman J. A., Goodrich C. A. and Wilson L. (2009) Metal and siderophile elements in ureilites: reconciliation with smelting? 40th *Lunar and Planetary Science Conference*, Abstract #1986.

Van Orman J. A. and Hayden L. A. (2011) A model for trace element partitioning in metallic systems containing multiple light elements. 42nd Lunar and Planetary Science Conference, Abstract #2367.

Walker R. J., McDonough W. F., Honesto J., Chabot N. L., McCoy T. L., Ash R. D. and Bellucci J. J. (2008) Modeling fractional crystallization of group IVB iron meteorites. *Geochim. Cosmochim. Acta* **72**, 2198–2216.

Wang C., Hirama J., Nagasaka T. and Ban-ya S. (1991) Phase equilibria of liquid Fe–S–C ternary system. *ISIJ Int.* **31**, 1292–1299.

Warren P. H. and Kallemeyn G. W. (1992) Explosive volcanism and the graphite–oxygen fugacity buffer on the parent asteroid(s) of the ureilite meteorites. *Icarus* **100**, 110–126.

Warren P. H., Ulff-Møller F., Huber H. and Kallemeyn G. W. (2006) Siderophile geochemistry of ureilites: a record of early stages of planetesimal core formation. *Geochim. Cosmochim. Acta* **70**, 2104–2126.

Wasson J. T. and Wai C. M. (1976) Explanation for the very low Ga and Ge concentrations in some iron meteorite groups. *Nature* **261**, 114–116.

Wasson J. T., Chou C.-L., Bild R. W. and Baedecker P. A. (1976) Classification of and elemental fractionation among ureilites. *Geochim. Cosmochim. Acta* **40**, 1449–1458.

Watson H. C. and Watson E. B. (2003) Siderophile trace element diffusion in Fe–Ni alloys. *Phys. Earth Planet. Int.* **139**, 65–75.

Wood B. J. (1993) Carbon in the core. *Earth Planet. Sci. Lett.* **117**, 593–607.

Associate editor: Alan D. Brandon